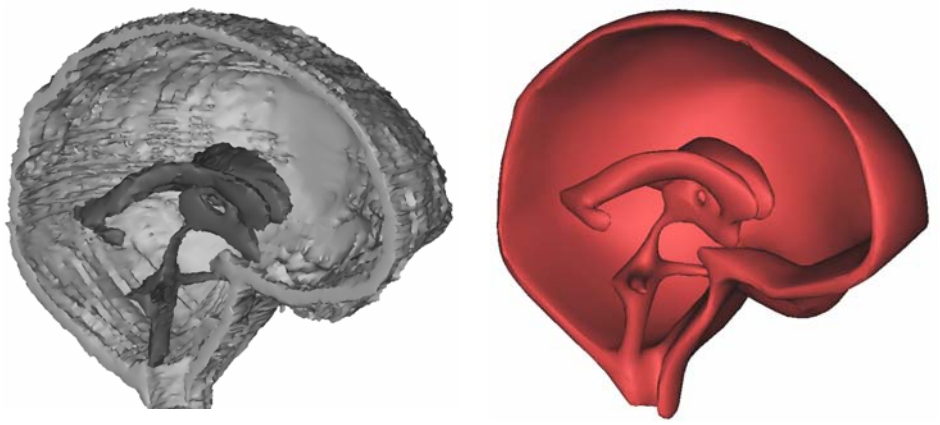

Figure 1: Manual segmentation of the CSF-filled spaces of the cranium resulted in the initially crude surface shown on the left. Advanced filtering techniques such as surface smoothing and triangle reduction resulted in the improved, more realistic surface displayed on the right.

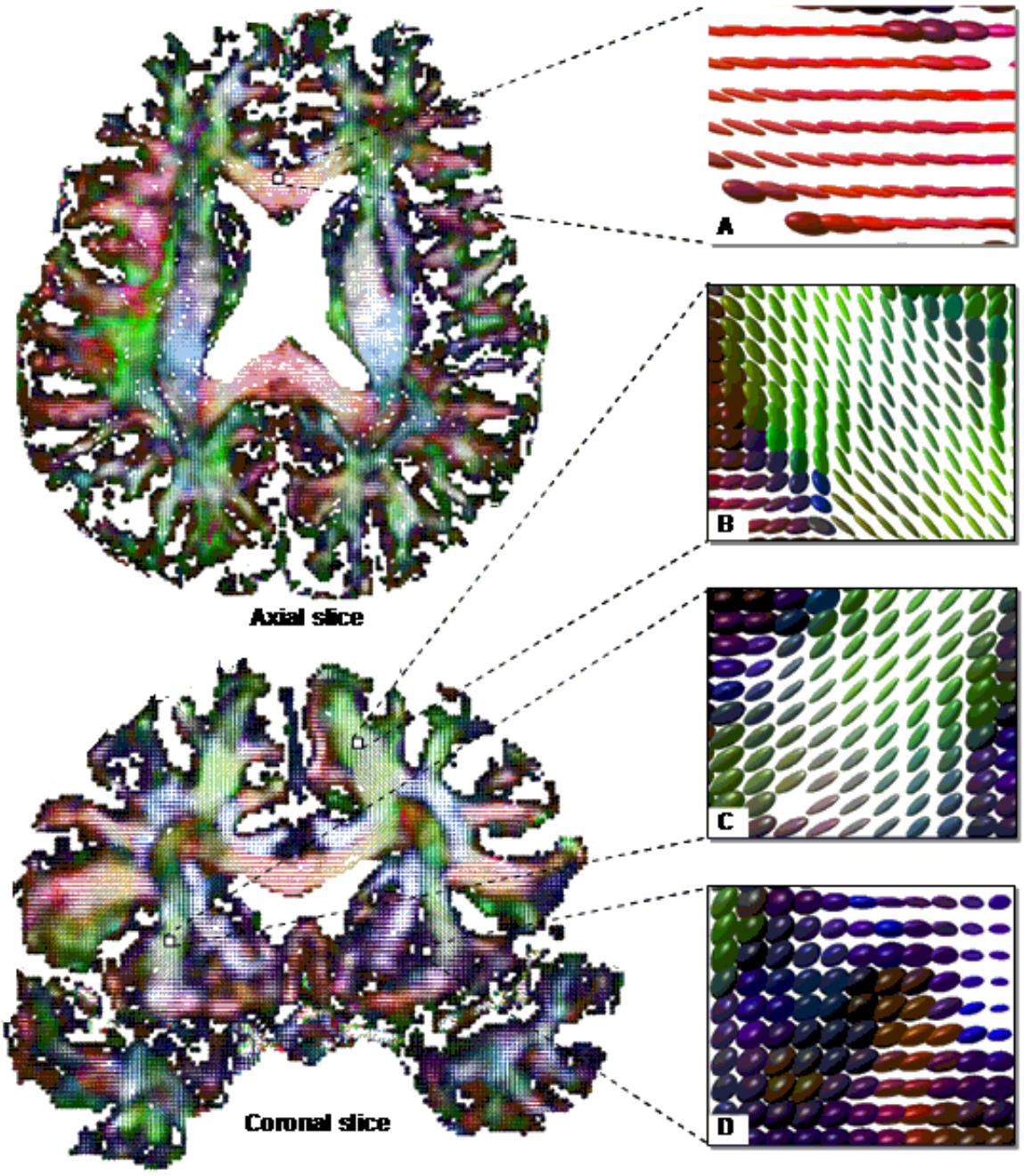

Figure 2: Axial and coronal DTI measurements for a 38 year old normal subject showing anisotropy and brain tissue heterogeneity. The local diffusion tensor in each voxel of axial and coronal brain sections is represented by an ellipsoid. Four sample locations - (A) corpus callosum, (B) corona radiata, (C) internal capsule, and (D) gray matter regions show the orientation of apparent water diffusion tensor ellipsoids in more detail.

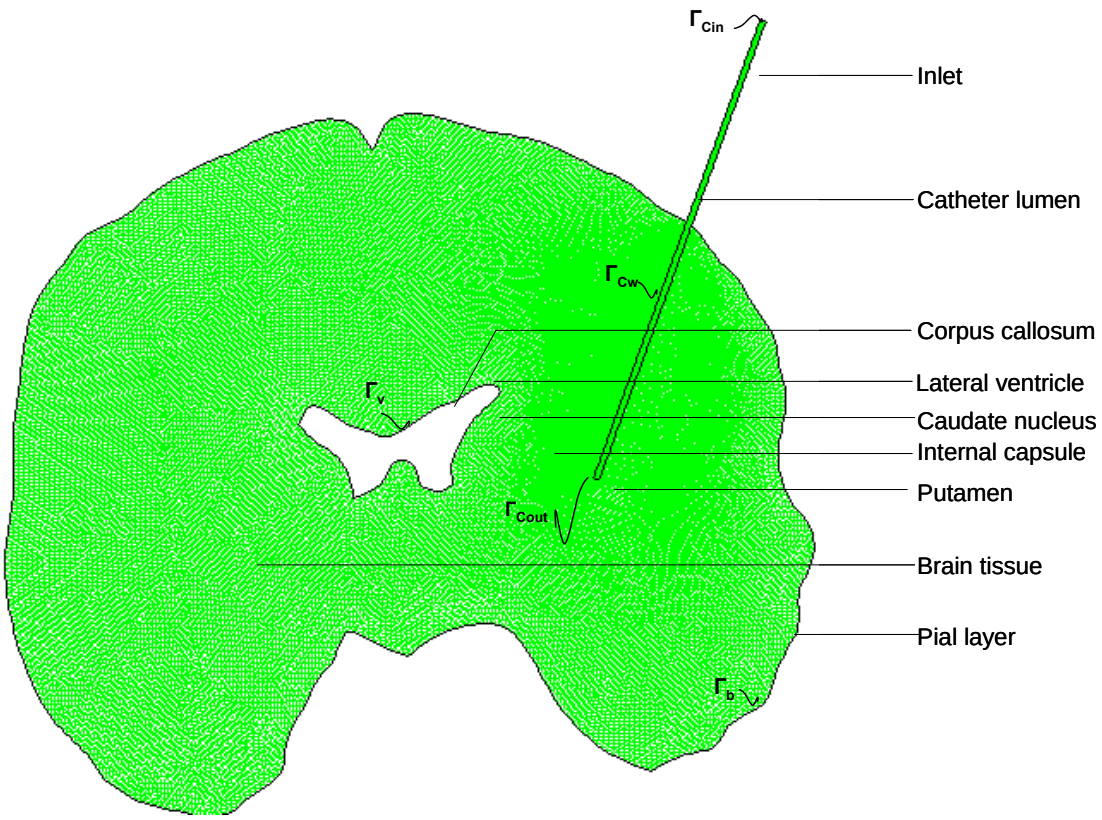

Figure 3: Two-dimensional computational mesh of a coronal human brain section with infusion catheter depicting the location of the boundaries (Γ_v, Γ_b, Γ_{Cin}, Γ_{Cw}, Γ_{Cout}) in which the boundary conditions are applied for predicting drug distribution with *iCFD* methods.

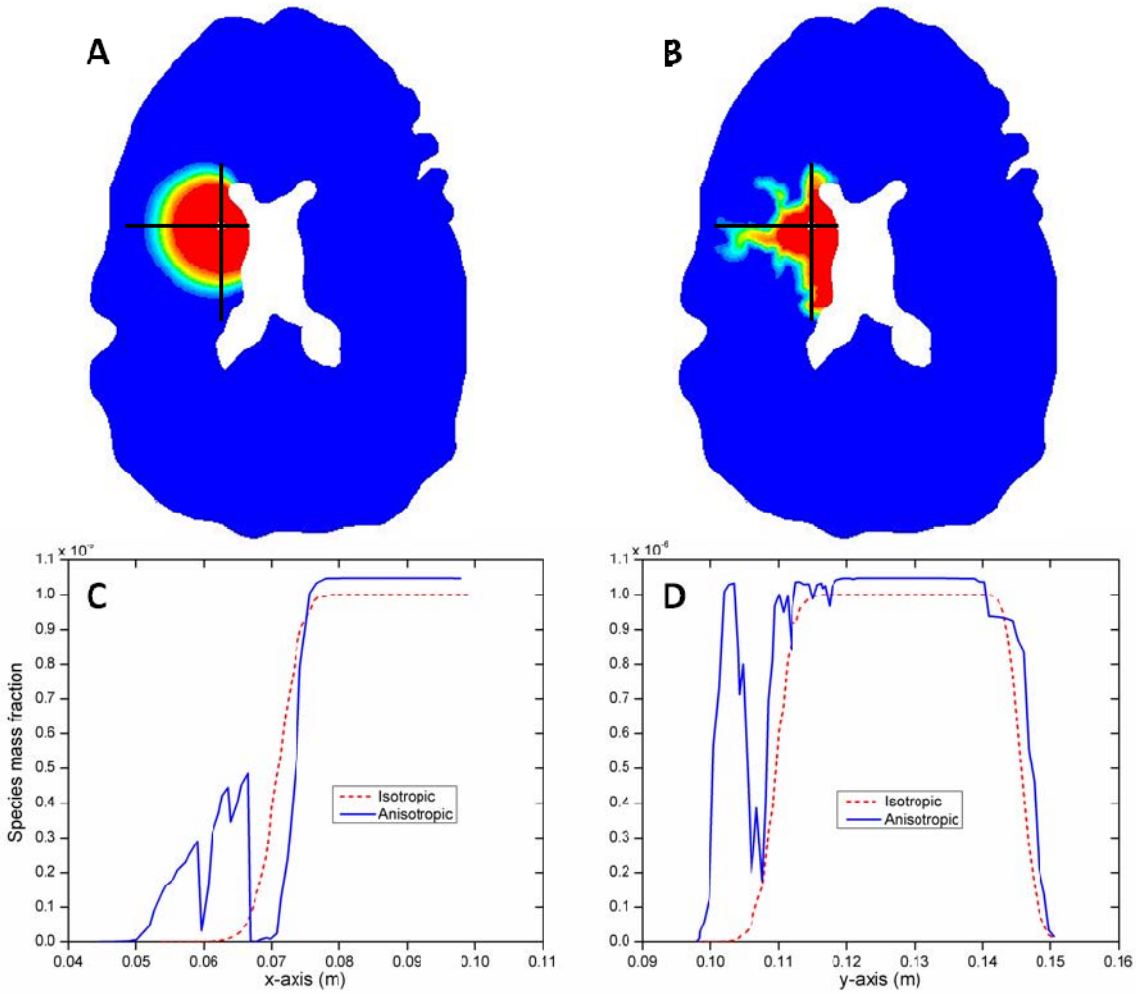

Figure 4: Axial brain section depicting the steady state CED distribution of a Nerve Growth Factor (NGF). Frame A shows a homogenous isotropic brain tissue model, frame B depicts results obtained using anisotropic heterogeneous DTI data. The anisotropic DTI model renders more realistic distribution pattern along white matter fiber tracts. Frame C and D compare the concentration profiles in x and y direction showing that the homogenous model may over or underestimate the anisotropic case.

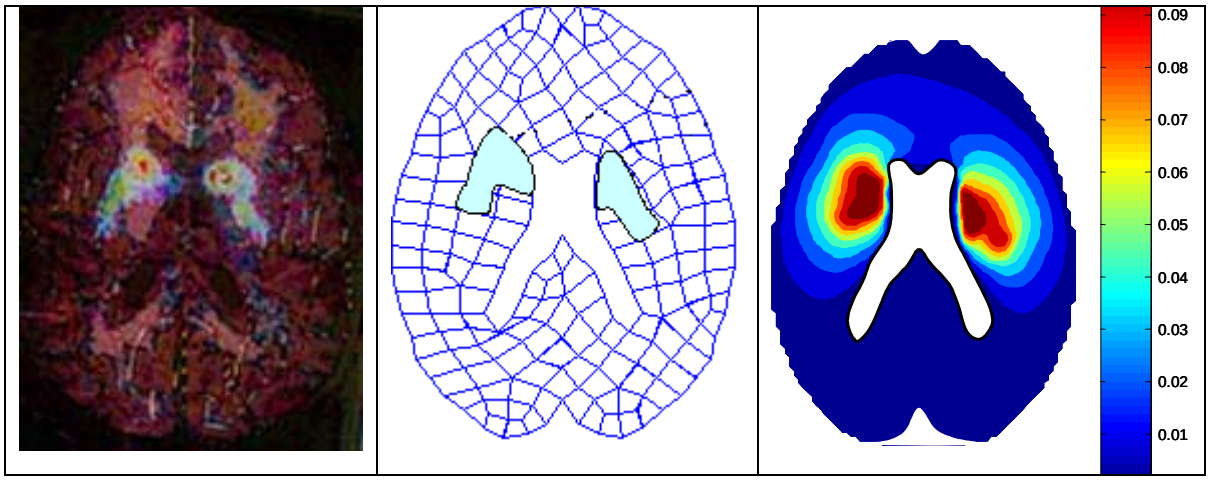

(a) The experimental data (b) The unstructured computational grid (c) Parameters projection with iterations

Figure 5 The results of solving a transport and kinetic inversion problem (TKIP) to estimate reaction rates and diffusivities of F-Dopa and methyl-F-dopa